

SDR-GAIN: A High Real-Time Occluded Pedestrian Pose Completion Method for Autonomous Driving

Honghao Fu, Libo Sun, Yilang Shen, Yiwen Wu

Abstract—To mitigate the challenges arising from partial occlusion in human pose keypoint based pedestrian detection methods, we present a novel pedestrian pose keypoint completion method called the separation and dimensionality reduction-based generative adversarial imputation networks (SDR-GAIN). Firstly, we utilize OpenPose to estimate pedestrian poses in images. Then, we isolate the head and torso keypoints of pedestrians with incomplete keypoints due to occlusion or other factors and perform dimensionality reduction to enhance features and further unify feature distribution. Finally, we introduce two generative models based on the generative adversarial networks (GAN) framework, which incorporate Huber loss, residual structure, and L1 regularization to generate missing parts of the incomplete head and torso pose keypoints of partially occluded pedestrians, resulting in pose completion. Our experiments on MS COCO and JAAD datasets demonstrate that SDR-GAIN outperforms basic GAIN framework, interpolation methods PCHIP and MAkima, machine learning methods k-NN and MissForest in terms of pose completion task. Furthermore, the SDR-GAIN algorithm exhibits a remarkably short running time of approximately 0.4ms and boasts exceptional real-time performance. As such, it holds significant practical value in the domain of autonomous driving, wherein high system response speeds are of paramount importance. Specifically, it excels at rapidly and precisely capturing human pose key points, thus enabling an expanded range of applications for pedestrian detection tasks based on pose key points, including but not limited to pedestrian behavior recognition and prediction.

Index Terms—pedestrian detection, occlusion, autonomous driving, GAN.

I. INTRODUCTION

In the context of traffic, pedestrians are considered one of the most challenging participants to predict, and a considerable number of traffic accidents occur annually due to non-compliance with traffic rules and carelessness on the part of both drivers and pedestrians [1]. One of the primary

objectives of autonomous driving is to enhance transportation safety and efficiency [2], decrease the incidence of traffic accidents [3], and alleviate traffic congestion [4]. In order to achieve this objective, pedestrian detection technology can be deployed during the autonomous driving process to enable pedestrian tracking [5] [6], behavior recognition [7] [8], and action prediction [9] [10]. These techniques can assist drivers in taking appropriate measures based on specific pedestrian scenarios or help autonomous driving systems to plan real-time paths accurately to avoid pedestrian collisions [11]. Hence, pedestrian detection represents an essential research direction in the field of autonomous driving [12].

Due to the remarkable progress achieved in electronic technology, computer science and artificial intelligence, contemporary pedestrian detection methods have demonstrated impressive performance and practical value, along with significant potential for further development. We broadly categorize pedestrian detection methods into the following categories: (1) traditional computer vision-based methods [13]-[15], which leverage traditional image features to recognize pedestrians. Although these methods possess mature theories and high reliability, they struggle to capture the underlying features of complex and variable situations, requiring significant human intervention and correction to adapt to different application scenarios. (2) Deep learning and computer vision-based methods [16]-[18] use deep neural networks to automatically learn video or image features to achieve pedestrian detection. They offer higher accuracy and better generalization by autonomously learning deeper levels of information within images. However, their model interpretability is poor, and high-quality datasets are required for training. (3) Non-visual physical sensor-based methods [19]-[21] detect pedestrians using sensors such as LIDAR and ultrasonic sensors, among others. These methods are unaffected by lighting and background environments, resulting in more stable detection results. However, it has a smaller scope of detection, comes at a higher cost, and is susceptible to the impact of environmental elements such as rain, snow, smoke, and sensor installation conditions. (4) Fusion methods based on visual and non-visual physical sensors [22] [23] combine computer vision with a physical model established through non-visual sensing for pedestrian detection. While these methods offer higher accuracy and robustness, they come with complex data processing requirements, and hardware and

This work was supported by the Key R&D Program of Jiangsu Province under Grant BE2019311 and National key research and development program under Grant 2020YFB160070301. (*Corresponding author: Libo Sun*)

Honghao Fu, Libo Sun and Yiwen Wu are affiliated with the School of Instrument Science and Engineering, Southeast University, Nanjing, China. Honghao Fu is also with the School of Electrical and Electronic Engineering, Nanyang Technological University, Singapore. (e-mail: HFU006@e.ntu.edu.sg)

Yilang Shen is affiliated with the School of Geospatial Engineering and Science, Sun Yat-sen University.

system maintenance costs are high. Since the deep learning and computer vision-based methods do not require manual design of image feature extraction and exhibit strong generalization ability after being trained on large-scale datasets [24], they demonstrate excellent performance in pedestrian detection and currently represent one of the most prominent research directions.

In the domain of autonomous driving, pedestrian detection possesses a practical significance owing to the fast speed of vehicles, complex and dynamic road conditions, numerous unpredictable factors, and severe consequences of traffic accidents involving pedestrians. Vision-based pedestrian detection techniques have demonstrated excellent performance, but they still exhibit inadequacies in certain aspects. Specifically, detection accuracy is significantly compromised when pedestrians are partially obscured [26] [27], resulting in errors in pedestrian tracking, behavior recognition, and action prediction tasks. In actual driving scenarios, particularly in complex traffic environments, automatic driving systems need to handle images of partially obscured pedestrians due to the influence of visual sensors such as cameras' placement, other vehicles, vegetation or building environments. Deep learning-based pedestrian detection tasks, such as action prediction and behavior recognition, typically employ either the entire image [28] or human body pose keypoints [29] as inputs for their models. Nevertheless, methods based on human body pose keypoints could lead to considerable errors in the final results if some keypoints are missing, thereby limiting the method's practical value and reliability. Moreover, the use of deep neural networks to process images often suffers from real-time performance limitations, which further constrains the application of some autonomous driving visual techniques[25].

In this paper, we introduce a novel method for completing missing pedestrian pose keypoints called Separation and Dimensionality Reduction-based Generative Adversarial Imputation Networks (SDR-GAIN) by integrating computer vision and deep learning techniques. The aim of this approach is to address the challenges posed by partial occlusion in existing pedestrian detection methods based on human body pose keypoints. SDR-GAIN generates missing coordinate data of keypoints through deep learning methods based on 2D human body pose estimation. To evaluate the effectiveness of SDR-GAIN in completing missing pedestrian pose data with good performance and high real-time capabilities, we conducted experiments on the Microsoft Common Objects in COntext (MS COCO) dataset and the Joint Attention in Autonomous Driving (JAAD) dataset. The experimental results demonstrate that SDR-GAIN has fast processing speed and high real-time capabilities while exhibiting excellent ability to complete missing pedestrian pose data.

II. RELATED WORKS

A. Pedestrian pose estimation methods

In order to obtain precise pedestrian pose data for decision-making or to complete the pose of occluded pedestrians, accurate estimation of pedestrian keypoints is

crucial. However, considering that traffic scenes typically involve numerous pedestrians, the top-down posture estimation method [30], [31], which is suitable for multiple individuals, has limited real-time performance. In this regard, the bottom-up method [32] can be adopted instead. Wei *et al.* [33] proposed a sequential convolutional structure model that systematically learned and expressed spatial information, acquired image features, and relied on an image spatial model for structured prediction tasks, implicitly simulating long-range dependencies between variables in human pose estimation. Cao *et al.* [34] introduced OpenPose, an effective method for detecting 2D human pose in images with multiple people. OpenPose employs the part affinity fields (PAFs) algorithm, where each detected body part is associated with its corresponding individual in the image and the global background is encoded. Additionally, a bottom-up parsing step is used to maintain high accuracy while achieving real-time performance. Cheng *et al.* [35] presented Higher HR Net, a bottom-up human pose estimation method based on learning scale-aware representations using a high-resolution feature pyramid network. The method uses multiple resolution supervisions for training and multiple resolution aggregations for inference, which better addresses the scale change problem in bottom-up multi-person posture estimation and enables more accurate keypoint localization, especially for small targets. With the continuous improvement of speed and accuracy in bottom-up methods for human pose estimation, they have great potential for autonomous driving applications.

B. Pedestrian detection tasks based on pose estimation

Posture-based methods are one of the pedestrian detection methods with potential for high application value in various areas, such as pedestrian behavior recognition [36], [37] and action prediction [38], [39]. In particular, Zhang *et al.* [40] proposed a human keypoint detection method to generate pedestrian skeleton keypoints from closed-circuit television (CCTV) videos and applied four machine learning models, including Support Vector Machine (SVM), Random Forest (RF), Gradient Boosting (GBM), and Extreme Gradient Boosting (XGBoost), to predict pedestrian intentions at red lights in intersections. Quintero *et al.* [41] introduced a novel approach for predicting pedestrian position and posture by utilizing the Balanced Gaussian Process Dynamical Model (B-GPDM) and Naive Bayes classifier with posture keypoints, enabling classification of intent 1 second in advance. Additionally, Fang and López [42] evaluated the effectiveness of using 2D posture estimation to detect pedestrian intentions under natural driving conditions using JAAD, which integrates CNN-based pedestrian detection, tracking, and posture estimation methods to predict crossing behavior from monocular images with excellent results. Cadena *et al.* [43] predicted pedestrian crossing intentions on urban roads based on two-dimensional human posture estimation and graph convolutional network (GCN). Furthermore, Marginean *et al.* [44] proposed a set of posture-based features and two recursive architectures, one with single output and the other with multiple outputs, for classifying short sequence images of different types

of pedestrian behaviors, such as standing or walking, crossing, accelerating, and waving.

Despite the high accuracy achieved by posture-based pedestrian detection methods with keypoints in their respective target tasks, the fixed number of keypoints used for further analysis may lead to partial missing due to occlusion or other problems. As a result, the inputs of conventional mathematical models, machine learning models, and deep neural network models employed in subsequent analyses may not be complete, ultimately impacting the final results. Materials and Methods.

C. Pose estimation of occluded pedestrians

Pedestrian detection methods are highly susceptible to performance degradation in the presence of occlusion, particularly under severe occlusion conditions [45]. Therefore, it is crucial to minimize the negative impact of occlusion on detection performance. Ouyang *et al.* [46] proposed a deep learning model that learns the visibility relationship between overlapping human poses, which can be utilized as a versatile post-processing method for pose estimation results. Mathias *et al.* [47] presented a cost-effective approach for training a set of classifiers for specific occlusion scenarios by reusing computations across various training stages. However, employing multiple classifiers trained for specific occlusion conditions leads to poor real-time performance due to high computational demands. Zhang *et al.* [48] introduced cross-channel attention mechanisms to represent various occlusion patterns within a single model and proposed an attention network with self- or externally-guided attention as an additional component to the baseline FasterRCNN detector for detecting occluded pedestrians. Kishore *et al.* [49] proposed ClueNet, a two-stage deep learning framework where the first stage generates visual cues for accurately estimating the poses of occluded pedestrians in the second stage. The first stage employs a multi-task network to segment visible parts and predict bounding boxes for visible and occluded regions surrounding each pedestrian. The second stage performs pose estimation using these predictions from the first stage. Nevertheless, this top-down approach still suffers from poor real-time performance, making it challenging to apply to autonomous driving.

Existing solutions to occlusion problems mostly rely on visual information, but image features of occluded pedestrians vary considerably depending on the occlusion pattern [48]. End-to-end solutions to occlusion problems are therefore difficult and lack versatility. More versatile methods, such as classifiers trained for specific occlusion conditions, are typically used as post-processing methods or additional components for pedestrian detection. Vision-based pedestrian detection methods incur significant computational demands and suffer from poor real-time performance. Consequently, relying solely on vision-based methods to address occlusion problems in autonomous driving may not be a practical solution.

D. Generative models

After conducting the above analysis, it is observed that

existing methods in the field of pedestrian detection have some limitations:

(1) Pose estimation and keypoint recognition-based methods exhibit good performance but have a high requirement for input keypoint data completeness. In the presence of occlusion, incomplete keypoint recognition can affect the generalization and practicality of such methods.

(2) Fully vision-based pedestrian detection methods use additional components to process occluded parts after basic detection, which typically results in significantly increased computational overhead that is unsuitable for real-time applications, such as autonomous driving.

In recent years, with the rapid development of generative models, new solutions have emerged to address the problem of missing keypoints in pose estimation. Goodfellow *et al.* [50] proposed a framework called generative adversarial networks (GAN) that uses an adversarial process to estimate generative models. This framework trains a generator to capture data distribution and a discriminator to determine if a sample comes from training data or the generator. Yoon *et al.* [51] adjusted the GAN framework and introduced generative adversarial imputation networks (GAIN), a novel method for estimating missing data using prompt vectors provided to the discriminator about the original sample's missing parts. The discriminator focuses on specific attribution qualities using this information to ensure the generator generates samples according to real data distribution. Ho *et al.* [52] were inspired by non-equilibrium thermodynamics and proposed an image generation method using diffusion probability models. They trained this model on a weighted variation constraint designed based on the new connection between the diffusion probability model and Langevin dynamics. Generative models' excellent performance in handling various types of missing data [53]–[55] validates their effectiveness.

Thus, in this study, the primary focus is to address the two gaps mentioned above using generative models, i.e., accurately completing pedestrian pose keypoints whenever possible, minimizing the negative impact caused by keypoint loss in pose estimation- and keypoint recognition-based pedestrian detection methods in the presence of occlusion, and overcoming the limitations of traditional vision-based methods for detecting occluded pedestrians with large computational overhead and poor real-time performance.

III. METHOD

A. Framework of SDR-GAIN

Figure 1 depicts the fundamental framework of the proposed method for completing missing poses of occluded pedestrians via pedestrian pose keypoint estimation and generation models. Initially, computer vision techniques grounded on deep learning can be applied to estimate pedestrian poses from images captured by cameras. The emergence of modern computer vision and deep learning techniques has provided sufficient theoretical backing for this task, with bottom-up multi-person pose estimation methods such as OpenPose [56] enabling efficient processing of data. Thereafter, incomplete

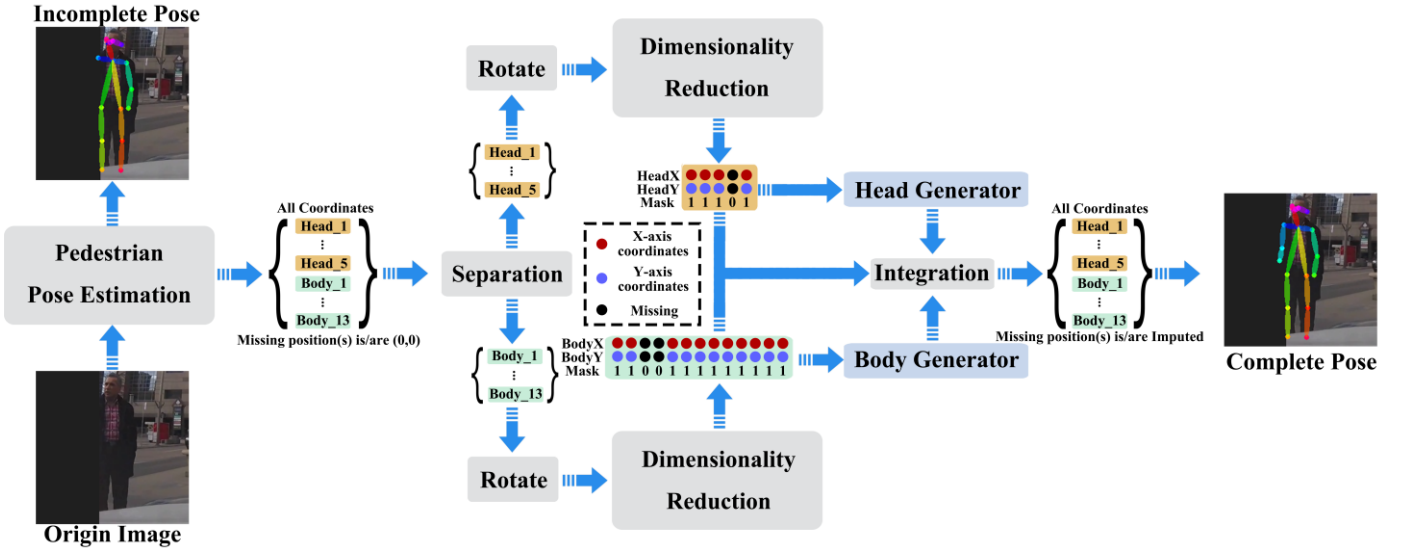


Fig. 1. Framework of SDR-GAIN.

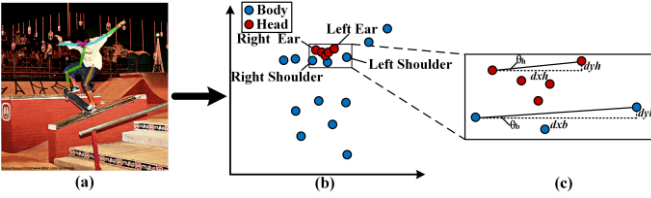


Fig. 2. Separation and calculation of rotation angle. (a) Image after pose estimation; (b) Corresponding coordinate map of keypoints, where blue dots represent keypoints of the torso and red dots represent keypoints of the head; (c) Calculation of rotation angle with reference to the right and left ears, and the right and left shoulders.

keypoints of pedestrians due to occlusion or other factors can be refined through separation and dimensionality reduction processing to unify their feature distribution, thereby facilitating better learning by neural networks. Finally, a trained generation model can be utilized to generate the missing parts of partial missing pedestrian pose keypoints, thus supplementing the missing poses of occluded pedestrians. This process involves initial estimation of pedestrian poses in a single image from a video using OpenPose. Subsequently, the head and torso keypoints that exhibit missing data are separated and rotated according to the right ear and left ear, and right shoulder and left shoulder as references to maximize the uniformity of horizontal and vertical distribution features. Two vectors indicating the missing position of head and body pose data serve as annotations for the missing data. Following this, the coordinates of the head and torso keypoints are reduced into one-dimensional distributions along the horizontal and vertical directions, respectively, and normalized to further enhance the uniformity of the distribution features. Additionally, the normalized projections of the head and torso keypoints are merged horizontally and vertically, respectively, and inputted simultaneously into two generation models along with their corresponding missing data annotation vectors for the generation of head and body pose data. These generation models utilize the GAN structure, trained with complete and

pre-processed pose data incorporating separation, rotation, and dimensionality reduction operations, and integrated with Hint mechanism to improve the performance of discriminators. Finally, the obtained data is restored through dimensionality expansion, rotation, and merging to derive coordinates in correspondence with the original image, thereby completing the poses.

B. Pedestrian pose estimation based on OpenPose

Pedestrian pose estimation aims to extract skeletal keypoints from the posture of pedestrians in each frame of an image or video, represented as a two-dimensional distribution, which facilitates subsequent analysis. OpenPose is a well-established and frequently used method for pedestrian pose estimation [57] [58], and has been widely adopted in research on autonomous driving [6] [59]. In this study, we utilized the classic 18-point model proposed by OpenPose based on the MS COCO 17-point model as the standard for pose estimation and completion. The model consists of five head keypoints representing the left eye, right eye, left ear, right ear, and nose, as well as thirteen body keypoints representing the left wrist, right wrist, left elbow, right elbow, left shoulder, right shoulder, left hip, right hip, left knee, right knee, left ankle, right ankle, and neck, where the neck is defined as the midpoint of the line connecting the left and right shoulders. Figure 2(a) presents the results of using OpenPose for pose estimation.

C. Separation and rotation

During pose estimation, the dispersion of head keypoints relative to torso keypoints is lower, as demonstrated in Figure 2(a), and there exists a notable distribution difference between them. Training both head and torso keypoints simultaneously in the neural network can result in less accurate feature learning by the network. To address this issue, it is necessary to extract the five head keypoints and thirteen body keypoints from the complete posture coordinate data and utilize them separately for training two GANs, which can generate distinct generators for absent keypoints of the head and torso, respectively. The

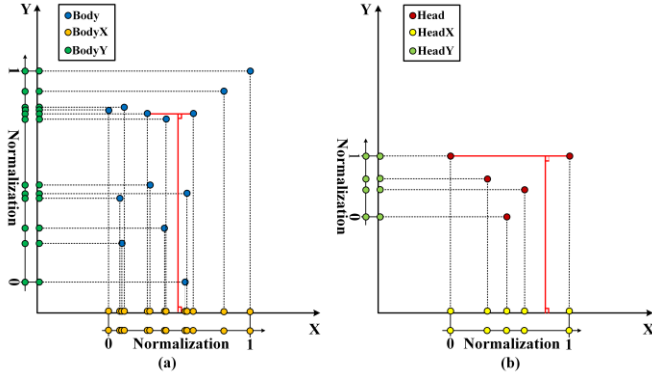


Fig. 3. Dimensionality reduction and normalization process. (a) Perform dimensionality reduction and normalization on the coordinates of the rotated keypoints of the torso. The blue coordinate point represents the two-dimensional coordinates, while the orange and dark green coordinate points represent their dimensionality reduced coordinates in the x and y directions, respectively; (b) Perform dimensionality reduction and normalization on the coordinates of the rotated keypoints of the head. The red coordinate point represents the two-dimensional coordinates, while the yellow and light green coordinate points represent their dimensionality reduced coordinates in the x and y directions, respectively.

specific separation of the keypoints marked in Figure 2(a) is presented in Figure 2(b). Human body postures in different images may have varying tilt angles, which cannot be intuitively reflected by the pure coordinate data format, leading to a potential impact on the distribution characteristics of the data. Hence, it is recommended to rotate the coordinate data before inputting it into the GAN to unify the distribution of keypoints as much as possible, thereby facilitating the learning of the neural network.

The set of coordinates for all keypoints in the head is denoted by H , where $H \in \mathbb{N}^2$. As depicted in Figure 2(c), the rotation center is chosen to be the right ear, specified by the coordinates (x_{hREar}, y_{hREar}) . The angle of rotation θ_h is defined as the acute angle formed between the line connecting the right ear and the left ear, specified by the coordinates (x_{hLEar}, y_{hLEar}) , and the x -axis. Moreover, dxh and dyh are defined as the distances between the two points in the x and y directions, respectively. It follows that:

$$\theta_h = \tan^{-1}\left(\frac{dyh}{dxh}\right) \quad (1)$$

Where $dxh = x_{hLEar} - x_{hREar}$, $dyh = y_{hLEar} - y_{hREar}$. Let B be a set of coordinates for all keypoints on the torso, where $B \in \mathbb{N}^2$. The rotation center will be the right shoulder point (x_{hRSh}, y_{hRSh}) . We define the acute angle formed by the line connecting the right and left shoulder points (x_{hLSh}, y_{hLSh}) with the x -axis as the rotation angle denoted by θ_b . Additionally, dxh and dyh represent the distance between the two points in the x and y directions, respectively. It follows that:

$$\theta_b = \tan^{-1}\left(\frac{dyb}{dxh}\right) \quad (2)$$

Where $dxh = x_{hLSh} - x_{hRSh}$, $dyh = y_{hLSh} - y_{hRSh}$.

Both the right eye and left eye, as well as the right ear and left ear, are situated on the same horizontal line. Nonetheless, to mitigate errors, we opt for the right ear and left ear as the reference points. Owing to the fact that images are made up of discrete pixels, the calculation of dxh and dyh involves an error of ± 1 pixel distance for both the right ear and left ear points. Consequently, this results in errors of ± 2 pixels for each of dxh and dyh . Let e_h denote the error in angle calculation:

$$e_h = \tan^{-1}\left(\frac{dyh \pm 2}{dxh \pm 2}\right) - \tan^{-1}\left(\frac{dyh}{dxh}\right) \quad (3)$$

In order to minimize errors, it is recommended to increase the values of dxh and dyh as much as possible. As a result, the keypoints of the right ear and left ear, which are further apart, are selected for use in this module. In the case of the trunk, the choice of using the right shoulder and left shoulder as the reference points is based on the strong correlation and limited range of motion between these two keypoints in the trunk. This makes them more suitable for accurately determining the tendency of the trunk posture.

D. Dimensionality reduction

We performed dimensionality reduction on the posture coordinate data by projecting each element of H and B onto the x and y axes and normalizing them, as illustrated in Figure 3. Specifically, Figure 3(a) shows the dimensionality reduction of keypoint coordinates for the torso, while Figure 3(b) shows the dimensionality reduction of keypoint coordinates for the head. The red lines in the figure indicate that the torso and head were rotated to a specified position before the dimensionality reduction process. The training set for the coordinate data is denoted as $S \in \mathbb{R}^3$, and we define the vector projections of the reduced torso and head keypoints in the x and y directions corresponding to the d -th image's coordinate data S_d as $B_{xd}, B_{yd}, H_{xd}, H_{yd} \in \mathbb{R}$, respectively. Due to rotation, the coordinate data is no longer integer pixels and may be negative, thus requiring definition in the real field. Furthermore, we define $S_d = \{B_{xd}, B_{yd}, H_{xd}, H_{yd}\} \in \mathbb{R}^2$, and let $S_{d,i,k}$ denote the k -th element of the i -th vector $S_{d,i}$ in S_d . We then define NS_d as the set of all elements in S_d after normalization and normalize all elements in $S_{d,i}$ based on the following formula:

$$NS_{d,i,k} = \frac{S_{d,i,k} - \min(S_{d,i,k})}{\max(S_{d,i,k}) - \min(S_{d,i,k})} \quad (4)$$

Where $NS_{d,i,k}$ represents the k -th component of the i -th vector $NS_{d,i}$ belonging to the set NS_d , where $NS_{d,i} \in [0,1]^k$. The primary objective of normalization is to map data that follow diverse distributions to the interval $[0,1]$, thereby standardizing the probability distribution characteristics and reducing the impact of anomalous sample data. This normalization process is particularly advantageous for GAN training and generating missing postures.

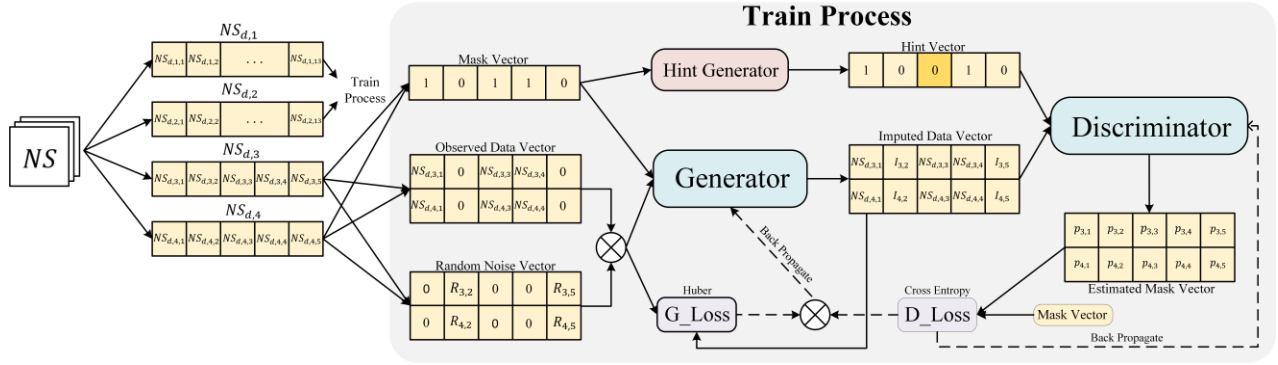


Fig. 4. The training process of generators and discriminators.

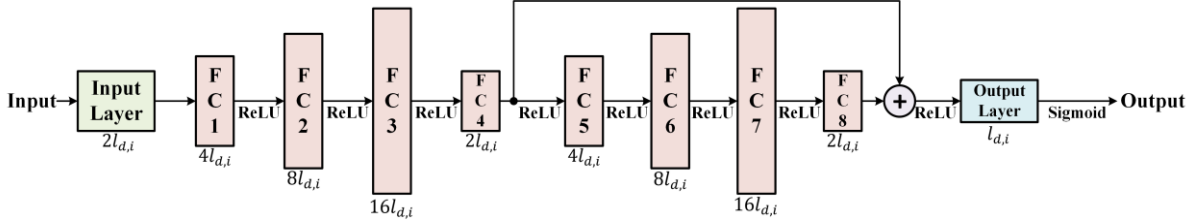


Fig. 5. Network structure.

E. Training of generators

GAN is a widely-used deep learning model framework that encompasses two neural networks, namely the generator and discriminator [50]. The generator utilizes input data to learn its probability distribution and subsequently generates synthetic data that closely resemble the training data. On the other hand, the discriminator determines whether input data is real or generated by evaluating whether it was part of the training data. These two networks engage in an antagonistic process where the generator attempts to deceive the discriminator with its generated data, while the discriminator strives to accurately differentiate between real and fake data. Through iterative optimization, the generator progressively generates more realistic data. GAIN [51], an advanced framework derived from adjusting the GAN structure, has demonstrated promising performance in missing data imputation [60] [61]. Nonetheless, human posture features clear two-dimensional spatial distribution characteristics, and the keypoints exhibit interdependence rather than merely following a simple data distribution. As such, abstracting two-dimensional distribution features and their correlations from coordinate data is a relatively complex task. Thus, we draw upon the GAIN framework for further research. To enable GAN to learn more abstract features from posture after dimensionality reduction, we appropriately deepen the neural network by introducing residual structures [62]. This approach allows certain layers of the neural network to bypass connections with the next layer of neurons and instead connect to deeper layers, thereby attenuating the strong correlations between each layer and preventing potential degradation issues. Additionally, regularisation processing is utilised to avoid overfitting. Our research plan details the specific training process of the generator and discriminator, which is shown in Figure 4.

First, the posture vectors that were obtained through

separation and dimensionality reduction are treated as distinct datasets for training the neural network. The same procedure is implemented to train each vector. Let p_m represents the rate of data loss, where $p_m \in (0,1)$. The length of vector $NS_{d,i}$ is $l_{d,i}$, and its corresponding mask vector is $M_{d,i} \in \{0,1\}^{l_{d,i}}$. Specifically, the k -th data point of $M_{d,i,k}$ can be defined as:

$$M_{d,i,k} = \begin{cases} 1, & \text{if } A_k > p_m \\ 0, & \text{Otherwise.} \end{cases} \quad (5)$$

Where A_k denotes a randomly-generated vector of length $l_{d,i}$, wherein the k th data point belongs to the vector $A \in [0,1]^{l_{d,i}}$. Moreover, it is important to note that each element in $M_{d,i}$ comprises specific pose keypoint information. Specifically, an element with a value of 1 conveys that the corresponding keypoint is not missing, whereas an element with a value of 0 indicates that the corresponding keypoint is missing. In addition, $M_{d,i}$ should satisfy the condition $M_{d,1} = M_{d,2}, M_{d,3} = M_{d,4}$.

Assuming that the observed data vector, after being masked, can be represented as $OS_{d,i}$, data at its k -th position is given by:

$$OS_{d,i,k} = \begin{cases} NS_{d,i,k}, & \text{if } M_{d,i,k} = 1 \\ 0, & \text{Otherwise.} \end{cases} \quad (6)$$

Assuming that $NR \in [0,1]^{l_{d,i}}$ is a random noise vector with a length of $l_{d,i}$, the corresponding interpolated random noise vector for $NS_{d,i}$ can be denoted as $R_{d,i}$ and is defined as follows:

$$R_{d,i} = (1 - M_{d,i}) \cdot NR \quad (7)$$

Figure 5 shows the structure of the generator and discriminator. To enhance the learning of posture features, we have made appropriate adjustments to the generator and discriminator while introducing residual structures. The generator, denoted as G, comprises hidden layers consisting of

eight fully connected layers that utilize ReLU as the activation function and contain residual modules. Each layer is defined by its input and output dimensions, with the eight fully connected layers structured as $(2l_{d,i}, 4l_{d,i})$, $(4l_{d,i}, 8l_{d,i})$, $(8l_{d,i}, 16l_{d,i})$, $(16l_{d,i}, 2l_{d,i})$, $(2l_{d,i}, 4l_{d,i})$, $(4l_{d,i}, 8l_{d,i})$, $(8l_{d,i}, 16l_{d,i})$, and $(16l_{d,i}, 2l_{d,i})$. Following the eighth fully connected layer, we employ a residual structure in which the output of the fourth layer is added to that of the eighth layer, and this combined output is then fed into an output layer that applies Sigmoid as the activation function.

The definition of $IS_{d,i}$ is given by $IS_{d,i} = OS_{d,i} + R_{d,i}$. IS_d is constructed by concatenating two non-repeating $IS_{d,i}$ with $i \in \{1, 2\}$ or $i \in \{3, 4\}$. Treating G as a function, we use IS_d and $M_{d,i}$ as inputs to obtain the predicted output $IG_d \in [0, 1]^{2l_{d,i}}$ after interpolating the missing data, which represents the generated prediction values. This process can be expressed as:

$$IG_d = G(IS_d, M_{d,i}) \quad (8)$$

Where IG_d is formed by concatenating two non-repeating $IG_{d,i}$, while adhering to the same i value present in $IS_{d,i}$ that constitutes IS_d . In the subsequent step, the non-missing data is superimposed onto the corresponding positions in the matrix $IG_{d,i}$, resulting in a novel vector $I_{d,i}$ where the k -th data point is denoted as $I_{d,i,k}$. This process can be represented as follows:

$$I_{d,i,k} = \begin{cases} NS_{d,i,k}, & \text{if } M_{d,i,k} = 1 \\ IG_{d,i,k}, & \text{Otherwise.} \end{cases} \quad (9)$$

The hint vector is generated by the hint generator, and its generation process is similar to that of $M_{d,i}$. Let C_k be the k -th data point in a random vector $C \in [0, 1]^{l_{d,i}}$ with a length of $l_{d,i}$. Let $p_h \in (0, 1)$ be the hint rate, and let the hint vector be $H_{d,i} \in [0, 1]^{l_{d,i}}$ where the k -th data point is denoted as $H_{d,i,k}$. The expression for $H_{d,i,k}$ is given by:

$$H_{d,i,k} = \begin{cases} M_{d,i,k}, & \text{if } C_k > 1 - p_h \\ 0, & \text{Otherwise.} \end{cases} \quad (10)$$

Furthermore, it is required that $H_{d,i}$ satisfy the condition $H_{d,1} = H_{d,2}$, $H_{d,3} = H_{d,4}$. Let D denote the discriminator, which has an architecture identical to that of the generator. I_d is formed by concatenating two non-repeating $I_{d,i}$ values, where $i \in \{1, 2\}$ or $i \in \{3, 4\}$. Treating D as a function, we use I_d and $H_{d,i}$ as inputs to D , resulting in an output $E_d \in [0, 1]^{2l_{d,i}}$, where the value of E_d represents the confidence that the generated data is real. This process can be expressed as:

$$E_d = D(I_d, H_{d,i}) \quad (11)$$

In order to train the discriminator D and the generator G using error backpropagation, loss functions need to be designed for each of them. Let $\mathcal{L}_D(a, b)$ denote the loss function for D . To measure the difference between the distribution of the generated data and the distribution of real data, cross-entropy is adopted as the loss function for D . Its basic form $\mathcal{L}_{CE}(a, b)$ is expressed as follows:

$$\mathcal{L}_{CE}(a, b) = -(b \log a + (1 - b) \log(1 - a)) \quad (12)$$

Let M_d be formed by concatenating two non-repeating $M_{d,i}$, while adhering to the same i value present in $E_{d,i}$ that constitutes E_d . Let the k -th element of E_d and M_d be denoted as $E_{d,k}$ and $M_{d,k}$, respectively. Let $a = E_{d,k}$ and $b = M_{d,k}$ in $\mathcal{L}_D(a, b)$, and rewrite equation (12) as:

$$\mathcal{L}_{CE}(E_{d,k}, M_{d,k}) = -(M_{d,k} \log E_{d,k} + (1 - M_{d,k}) \log(1 - E_{d,k})) \quad (13)$$

By averaging the $\mathcal{L}_{D,k}$ values across all bits in a given input sample, we arrive at the loss function \mathcal{L}_D for dataset D with respect to the current input sample:

$$\mathcal{L}_D(E_d, M_d) = \frac{1}{2l_{d,i}} \sum_{k=1}^{2l_{d,i}} \mathcal{L}_{CE}(E_{d,k}, M_{d,k}) \quad (14)$$

The loss function described here plays an important role in the training process of the D . Specifically, when $M_{d,k} = 1$, the output $E_{d,k}$ represents the confidence score of D when real data is used as input. The goal is to have D correctly identify the real data as such, and thus we aim to maximize $E_{d,k}$ towards 1, which in turn minimizes $-\log E_{d,k}$. Conversely, when $M_{d,k} = 0$, the output $E_{d,k}$ represents the confidence score of D when generated data is used as input. Here, the objective is for D to correctly identify the generated data as fake, and hence we aim to minimize $E_{d,k}$ towards 0, which in turn minimizes the expression $-\log(1 - E_{d,k})$. Through this iterative process, we can effectively train the D . Let the length of the coordinate dataset S be represented by l_s . Then, the training procedure of D can be summarized as follows:

$$\min_D \sum_{d=1}^{l_s} \mathcal{L}_D(E_d, M_d) \quad (15)$$

To train the D , updates are made through stochastic gradient descent (SGD).

$$\nabla_D \sum_{d=1}^{l_s} \mathcal{L}_D(E_d, M_d) \quad (16)$$

Then the latest update of D is utilized to train G . As the output of G includes not only generated values at missing data points but also new values obtained through neural network processing at non-missing data points, solely evaluating the discrepancy between generated and actual values at missing data points is inadequate for G to acquire knowledge regarding the distribution of authentic data. Consequently, it becomes necessary to evaluate the degree of similarity between new values at non-missing data points and their original counterparts. Firstly, in light of the most recent D update, the loss function \mathcal{L}_M is defined as below to assess the quality of generated values at missing data points:

$$\mathcal{L}_M(E_d, M_d) = -\frac{1}{2l_{d,i}} \sum_{k=1}^{2l_{d,i}} (1 - M_{d,k}) \log(E_{d,k}) \quad (17)$$

During the process of model training using gradient descent,

mean squared error (MSE) is generally more accurate than mean absolute error (MAE). However, when outliers are present, MAE exhibits better robustness than MSE. Therefore, we chose the Huber loss function to evaluate the similarity between generated values and true values at non-missing positions. The basic form of the Huber loss function is given below:

$$\mathcal{L}_{Huber}(y, f(x)) = \begin{cases} 0.5(y - f(x))^2 & , \text{ if } |y - f(x)| \leq \delta \\ \delta|y - f(x)| - 0.5\delta^2 & , \text{ Otherwise.} \end{cases} \quad (18)$$

In the given equation, δ corresponds to a hyperparameter. When the prediction deviation is less than or equal to δ , the Huber loss tends to be equivalent to MAE; whereas if it exceeds δ , it tends to be equivalent to MSE. To accurately reflect the performance of the generator in learning the true data distribution, the loss should be computed using data that is not been marked missing. This requires introducing a variable, denoted as m , which represents the mask vector. Therefore, we define $\mathcal{L}_{Huber}(y, f(x), m)$ as the Huber loss used by the generator G . Let the k -th element of IS_d and IG_d be denoted as $IS_{d,k}$ and $IG_{d,k}$, respectively. By setting $y = IS_d$, $f(x) = IG_d$, and $m = M_d$, we obtain the following equation:

$$\mathcal{L}_{Huber,k}(IS_d, IG_d, M_d) = \begin{cases} 0.5(IS_{d,k} - IG_{d,k})^2 M_{d,k}^2 & , \text{ if } |IS_{d,k} - IG_{d,k}| < \delta \\ \delta M_{d,k}(|IS_{d,k} - IG_{d,k}|) - 0.5\delta^2 & , \text{ Otherwise.} \end{cases} \quad (19)$$

$$\mathcal{L}_{Huber}(IS_d, IG_d, M_d) = \frac{\sum_{k=1}^{2l_d} \mathcal{L}_{Huber,k}(IS_d, IG_d, M_d)}{\sum_{i=1}^{2l_d} M_{d,k}} \quad (20)$$

In order to prevent overfitting, L1 regularization is employed in the current neural network. The penalty p is defined as the summation of the absolute values of all weights within the network, with λ being the corresponding penalty hyperparameter. Ultimately, the loss function \mathcal{L}_G of G with respect to the current input sample can be derived:

$$\mathcal{L}_G(IS_d, IG_d, M_d, E_d) = \alpha \mathcal{L}_{Huber}(IS_d, IG_d, M_d) + \mathcal{L}_M(E_d, M_d) + \lambda p \quad (21)$$

Where α is a hyperparameter. The fundamental objective of this loss function is to train generator G to produce data in the missing areas that can be convincingly distinguished as real by the discriminator D , given $M_{d,k} = 0$. This necessitates minimizing \mathcal{L}_M and maximizing $E_{d,k}$ to approach 1. Subsequently, when $M_{d,k} = 1$, we aim to minimize \mathcal{L}_{Huber} , such that the values generated by G in the non-missing areas are as similar as possible to the actual values. Adjusting the hyperparameter α offers control over the influence of \mathcal{L}_{Huber} on \mathcal{L}_G , thereby regulating the performance optimization of G . The training procedure of G can be summarized as follows:

$$\min_G \sum_{d=1}^{l_s} \mathcal{L}_G(IS_d, IG_d, M_d, E_d) \quad (22)$$

To train the G , updates are made through SGD:

$$\nabla_G \sum_{d=1}^{l_s} \mathcal{L}_G(IS_d, IG_d, M_d, E_d) \quad (23)$$

IV. EXPERIMENTS AND EVALUATIONS

A. Experimental platform and dataset

The hardware platform used in our experiment comprises of an RTX 3060Ti GPU, an i-7 12700F CPU, and 32GB of operating memory. The software platform mainly consists of PyCharm 2022.2.2 and Matlab R2023a. We trained and tested the SDR-GAIN model using the MS COCO and JAAD datasets. The MS COCO dataset is a general large-scale dataset that contains over 2.5 million labeled instances in 328,000 images [63], including keypoints annotations for more than 100,000 human bodies, and is a commonly used dataset to train pose estimators such as OpenPose. On the other hand, the JAAD dataset showcases the variability of behavior among traffic participants and is primarily employed in autonomous driving research [64]. Both MS COCO and JAAD have been extensively used in pedestrian pose estimation tasks. For instance, Fang and López [42] adopted pose estimators trained on the MS COCO dataset and conducted experimental verification on the JAAD dataset, which is the same as the research of Zhao *et al.* [65], which proposed a pedestrian crossing intention prediction method based on the ViT model. These studies provide conclusive evidence regarding the effectiveness of the datasets we utilized. Given the larger sample size, complex poses, and lower repeatability of the MS COCO dataset, we conducted ablation experiments primarily on this dataset to ensure that our method's generality and reliability are well-demonstrated by the experimental results. In contrast, since pedestrians are typically in a standing or walking state, the pose distribution in the JAAD dataset is relatively similar and closer to actual traffic scenarios despite its smaller sample size. Hence, we utilized the JAAD dataset and the MS COCO dataset for comparative experiments to validate the practical value of our approach in autonomous driving-related scenarios.

B. Objective evaluation of model performance

In order to investigate the factors that impact the performance of the SDR-GAIN keypoint completion method and determine the optimal solution, we conducted experimental analysis focusing on separation, dimensionality reduction, Huber loss function, and residual structure. We partitioned the coordinate dataset of human keypoints after pose estimation into a training set and a test set using an 8:2 ratio. Unless otherwise specified, the hyperparameters used in the method were set to default conditions as follows: mini batch size of 128, epochs of 5000, data loss rate $p_m = 0.2$ in equation (5), prompt rate $p_h = 0.9$ in equation (10), $\delta = 0.6$ in equation (18), and $\alpha = 10$ and $\lambda = 0.001$ in equation (21).

1) Sensitivity factors analysis

To assess the effectiveness of neural network training on a specific data type and determine the optimal training conditions for all data dimensions and their combinations following

Loss & Structure	SDR-GAIN						w/o DR		w/o S			w/o S & DR
	HeadD	HeadX	HeadY	BodyD	BodyX	BodyY	Head	Body	BothD	BothX	BothY	Both
MSE & Res	0.4527	0.1362	0.1834	0.3470	0.2281	0.2485	0.2233	0.1383	0.3537	0.1969	0.1972	0.2113
Huber & Res	0.4391	0.1441	0.1664	0.3341	0.2173	0.2309	0.1716	0.2046	0.3257	0.2265	0.2306	0.2260
MSE w/o Res	0.4351	0.1571	0.1797	0.3726	0.2375	0.2578	0.3576	0.2414	0.3434	0.2122	0.2377	0.2131
Huber w/o Res	0.4022	0.1318	0.1648	0.3559	0.2331	0.2505	0.1888	0.2768	0.3372	0.2321	0.2323	0.2271

Table 1. Performance of generator models with different structures under separation and dimensionality reduction (RMSE)

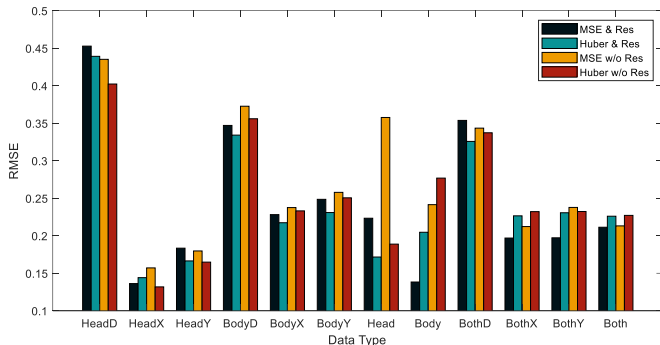


Fig. 6. Comparison of results in Table 1.

Loss & Structure	SDR-GAIN		w/o DR	w/o S		w/o S & DR
	Dev	NDev	—	Dev	NDev	—
MSE & Res	0.0401	0.0242	0.0839	0.0489	0.0454	0.0929
Huber & Res	0.0516	0.0240	0.0688	0.0373	0.0495	0.0794
MSE w/o Res	0.0334	0.0277	0.0665	0.0279	0.0420	0.0768
Huber w/o Res	0.0524	0.0256	0.0681	0.0387	0.0508	0.0792
Average	0.0444	0.0254	0.0713	0.0382	0.0469	0.0821

Table 2. Comprehensive performance evaluation of multi generator models fusion (RMSE).

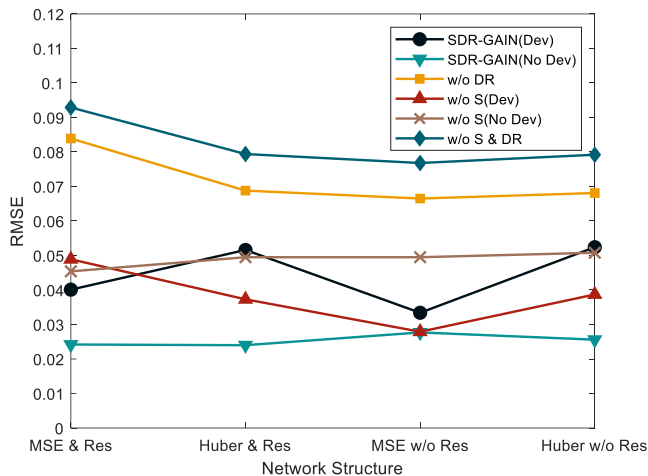


Fig. 7. Comparison of results in Table 2

separation and dimensionality reduction, we deployed our trained generator on the MS COCO testset, and observe the sensitive factors that affect model performance. We evaluated the performance of the generator by measuring the root mean

squared error (RMSE) between the generated results and real data normalized at the same scale during ablation experiments. Our findings are presented in Table 1, where we used "w/o" to indicate the removal of a particular module or network structure in SDR-GAIN. In this context, "S" refers to the separation module, "DR" denotes the dimensionality reduction module, while "MSE" and "Huber" represent the corresponding loss functions, and "Res" represents the residual structure. We defined "Head" and "Body" as data sets collected from the head and torso under separation, respectively. When not separated, "Both" represents the collection of all body keypoints. "HeadD," "BodyD," and "BothD" represent the corresponding data after dimensionality reduction based on separation. Due to the dimensionality reduction step's presence in the SDR-GAIN group, "HeadD" is composed of coordinate data "HeadX" and "HeadY" in the x-axis and y-axis directions after dimensionality reduction. Similarly, "BodyD" and "BothD" in the "w/o S" group consist of "BodyX," "BodyY," "BothX," and "BothY." Since the normalized scales of each dimension of data after separation differ, valid inter-group comparisons are not possible. Therefore, we compared the same data types under varied neural network structures to identify the most appropriate network structure for each data type.

The results from Table 1 and Figure 6 indicate that, in more cases, the use of Huber loss function and residual structures can optimize the performance of a neural network. However, it is noteworthy that for Head-related data in the SDR-GAIN group, the performance is relatively better without introducing residual structures. Moreover, when dealing with Body data in the w/o DR group, BothX and BothY data in the w/o S group, and data in the w/o S & DR group, the use of MSE as the loss function leads to better performance. Hence, it is crucial to consider the specific data characteristics before deciding whether to adopt the Huber loss function and residual structures, even though they can enhance the neural network's performance.

2) Multi generator models fusion

Multi-generator models fusion evaluation aims to evaluate the overall performance of different generator models that have been trained on separate datasets and deployed in parallel under similar training conditions. For instance, two generator models that have been trained on distinct datasets for the head and body are merged to analyze the output results for errors. To assess which method performs better overall, this study compared four methods - SDR-GAIN, w/o DR, w/o S, and w/o S & DR - under

Dataset Indicators		Interpolation Method					
		SDR-GAIN	GAIN	PCHIP	MAkima	k-NN	MissForest
COCO	RMSE	0.0225	0.0768	0.7788	0.7216	0.3406	0.3392
	Time/s	4.580×10^{-4}	1.128×10^{-4}	9.314×10^{-5}	4.635×10^{-5}	2.131×10^{-4}	3.560×10^{-3}
JAAD	RMSE	0.0117	0.0672	0.9486	0.8876	0.6171	0.5936
	Time/s	4.087×10^{-4}	1.077×10^{-4}	3.729×10^{-5}	3.461×10^{-5}	8.336×10^{-5}	7.824×10^{-3}

Table 3. Performance comparison between SDR-GAIN and other imputation algorithms

Indexes	Pedestrian Pose Estimation Task			
	PEN-AL	PEN-AL	PEN-	Cam
	FNet-1s	FNet-2s	CSP	Loc
Time/s	0.07	0.08	0.10	0.023
Proportion/%	0.57	0.50	0.40	1.74

Table 4. Running time of tasks about pedestrian pose estimation and relative proportion of SDR-GAIN’s time cost.

Number	Keypoint	Number	Keypoint
0	Nose	9	Right Knee
1	Neck	10	Right Ankle
2	Right Shoulder	11	Left Hip
3	Right Elbow	12	Left Knee
4	Right Wrist	13	Left Ankle
5	Left Shoulder	14	Right Eye
6	Left Elbow	15	Left Eye
7	Left Wrist	16	Right Ear
8	Right Hip	17	Left Ear

Table 5. Correspondence between numbers and keypoints

four network structures on the MS COCO test set, using RMSE as the primary measure of performance, as shown in Table 2. The SDR-GAIN group with "Dev" refers to the use of four generators to produce HeadX, HeadY, BodyX, and BodyY separately. Meanwhile, "No Dev" denotes the use of two generators to generate HeadD and BodyD, respectively. The w/o S group follows a similar pattern, where "Dev" means the use of two generators to generate BothX and BothY separately, while "No Dev" implies the direct utilization of one generator for generating BothD. For the w/o DR group, since dimensionality reduction was not employed, two generators were used to generate the head and body separately. In contrast, for the w/o S & DR group, neither separation nor dimensionality reduction was performed, hence only one generator was used directly to generate Both.

However, under comprehensive evaluation, it is necessary to normalize the head and body separately before inputting into SDR-GAIN. Due to a lack of consistent normalization scales, direct merging and calculation of RMSE is not possible. As such, conversion to real coordinates is required prior to normalizing all data in the dataset together to unify the normalization scale to the same size. This approach leads to smaller RMSE values, as shown in Table 2, but is still a key means of significantly evaluating the performance of each method.

Based on the data presented in Table 2 and Figure 7, it can be inferred that the No Dev group outperforms the other groups when evaluated using the SDR-GAIN method. Therefore, to achieve optimal performance when implementing the SDR-GAIN method, it is recommended to train two generator models, namely HeadD and BodyD. Moreover, both separation and dimensionality reduction stages contribute to the improved performance, with the former having a more significant impact. As training two generator models is necessary to attain optimal performance, it is essential to determine their respective optimal neural network structures by analyzing the data presented in Table 1. During the model training process, we recommend adopting Huber as the loss function for HeadD without introducing residual structure for training. On the other hand, for BodyD, we suggest using Huber as the loss function, along with introducing residual structure for training. This approach should be considered the standard method when employing SDR-GAIN.

3) Comparative experiment

We deployed the standard method of SDR-GAIN along with several other interpolation methods on separate MS COCO and JAAD test sets to compare their differences in accuracy and real-time performance for the task of completing human pose data. The comparison methods include not only the original GAIN framework but also widely used non-deep learning missing data filling methods such as the interpolation algorithms piecewise cubic Hermite interpolation polynomial (PCHIP) [66] and modified Akima piecewise cubic Hermite interpolation (MAkima) [67], machine learning algorithm k-nearest neighbors (k-NN) [68], and MissForest [69]. We used RMSE and running time as our comparison metrics and have presented the experimental data in Table 3. The running time refers to the average time taken to complete a human pose.

Based on the data presented in Table 3, it is evident that SDR-GAIN exhibits significantly superior accuracy compared to other interpolation algorithms when utilized for human pose completion tasks. Conventional interpolation algorithms like PCHIP and MAkima have limited efficacy when applied to human pose coordinate data. While machine learning algorithms such as k-NN and MissForest have shown promise in summarizing certain features of pose data based on their performance on the MS COCO dataset, there still exists a significant margin for error (with k-NN exhibiting an RMSE of 0.3406 and MissForest exhibiting an RMSE of 0.3392). On the other hand, deep learning methods like SDR-GAIN and GAIN

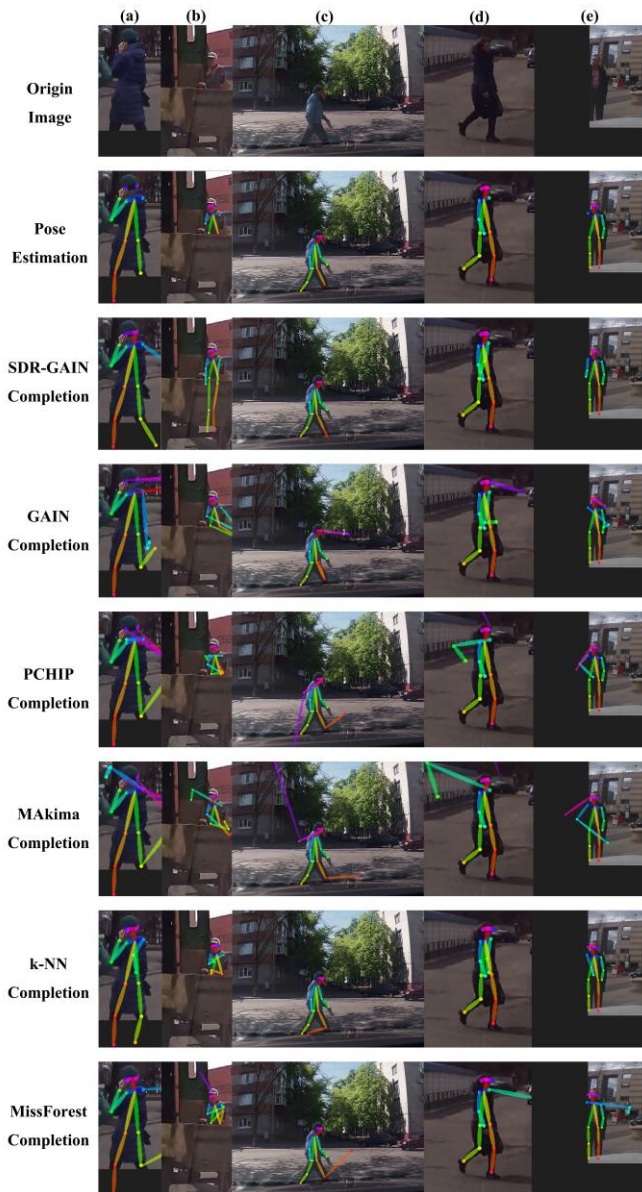


Figure 8: Comparison of the original image, OpenPose pose estimation, and pose completion results.

demonstrate relatively good performance, indicating that they are capable of effectively extracting essential pose data features from coordinate data. SDR-GAIN outperforms GAIN significantly in terms of interpolation performance, as observed in both the MS COCO and JAAD datasets, thus demonstrating its robust generality. Additionally, upon applying SDR-GAIN to the JAAD dataset, it proves to be more effective than MS COCO, highlighting its high potential in enabling pedestrian pose completion tasks for autonomous driving systems.

Although SDR-GAIN has the potential to increase computation time compared to other imputation algorithms, except for MissForest, its speed of approximately 0.4ms per posture completion is still deemed acceptable. Assuming a vehicle is traveling at a speed of 130 km/h [70], the posture completion process can be completed within a driving distance of 0.014m (1.4cm). We conducted an evaluation to determine

whether using SDR-GAIN as an additional post-processing module would affect the real-time performance of the original system. Table 4 presents the processing time required by an obscured pedestrian posture estimation method PEN [71] for a 480×640 image and the running time of another pedestrian location method CamLoc [72] based on pedestrian posture estimation. Moreover, we calculated the percentage of SDR-GAIN's running time (4ms) relative to the running time of these two methods.

Based on the data presented in Table 4, it can be observed that incorporating SDR-GAIN as a post-processing module does not result in any significant increase in the overall time when compared to the three branch schemes of relative PEN and the running time of CamLoc itself. Specifically, for PEN, the average increment is only 0.49%, while for CamLoc, the increment is 1.74%. Consequently, we contend that integrating the SDR-GAIN method as a post-completion module will not unduly impact the real-time performance of the original system, and it holds considerable practical value within the context of automatic driving applications.

C. Visualization of keypoints completion results

We conducted evaluations of the pose completion performance of SDR-GAIN by deploying it on the JAAD dataset and performing visual experiments, and compared the completion results of different interpolation methods. Figure 8 presents examples of pose completion before and after, with the exception of missing keypoints in the head. Specifically, in scenario (a), we observed missing foot and hand keypoints due to image boundary and self-occlusion problems. We completed keypoints 0, 3, 4, 10, 14, and 15 to address this issue. In scenario (b), large object occlusion caused severe trunk keypoint loss, where keypoints 4, 6, 7, 9, 10, 12, and 13 were completed. In scenario (c), the car hood resulted in missing foot keypoints, and we resolved this by completing keypoints 13, 15, and 17. Scenario (d) involved missing arm keypoints due to self-occlusion, and we completed keypoints 6, 7, and 17 as a remedial measure. Finally, scenario (e) had missing arm keypoints caused by an image boundary problem, which we addressed by completing keypoints 3, 4, and 16. Notably, the dark gray area in Figure 8 denotes regions that are beyond the image boundary. Further information regarding the numerical identifiers for each keypoint is available in Table 5.

Based on the results presented in Figure 8, it can be inferred that the SDR-GAIN method has the ability to approximately generate missing key points. Furthermore, the completed results obtained through SDR-GAIN are comparatively more accurate and realistic as compared to other interpolation algorithms. Moreover, we observed in experiments that when using random noise data to fill in a missing dimension, the generated missing points are more realistic subjectively as the noise data approaches the true value of the missing point. As a result, it could be beneficial to consider using the coordinate values of the nearest non-missing point instead of random noise data as input to the generator model for improved performance. The distance between these points can be quantified using the node distance of the graph structure transformed from the

human pose connection relationship, where each node corresponds to a keypoint. However, when multiple missing points exist, as illustrated in Figure 8(b), the nearest non-missing point might not be an adequate replacement for random noise data. Additionally, while normalizing data with missing keypoints, it is crucial to consider appropriately expanding the normalization interval. This is because if the known keypoints (corresponding to the Pose Estimation row) are directly normalized, as shown in Figure 8(b), the actual leg coordinates will surpass the value of 1 in that normalization scale, and the generator model can only provide output within the $[0, 1]$ range due to its output layer being a Sigmoid function, resulting in incorrect data generation.

V. CONCLUSIONS

This study presents an innovative method called SDR-GAIN, which combines computer vision and deep learning technologies for pedestrian pose keypoint completion. The proposed approach is tested on various datasets, demonstrating superior performance compared to other data interpolation methods for completing pedestrian poses. SDR-GAIN effectively generates approximate keypoints in missing postures with good real-time performance, making it suitable for autonomous driving applications. The research findings are summarized as follows:

(1) The proposed separation and dimensionality reduction steps enhance the expression of human pose keypoint features, facilitating the learning of the inherent connections in posture coordinate data by deep neural networks. The use of a dual-generator structure to process separated data improves accuracy. Additionally, incorporating Huber loss function, residual structure, and L1 regularization optimizes the GAN framework and improves network performance while mitigating degradation and overfitting issues.

(2) SDR-GAIN achieves an RMSE of 0.0225 on the MS COCO dataset and an RMSE of 0.0117 on the JAAD dataset for pedestrian pose keypoint interpolation, which significantly surpasses the basic GAIN framework, interpolation methods PCHIP and MAkima, and machine learning techniques k-NN and MissForest.

(3) The running time of SDR-GAIN is approximately 0.4ms under the experimental conditions. When used as an additional module for pedestrian pose estimation, it does not significantly impact overall system running time and exhibits good real-time performance in the field of autonomous driving.

Based on experimental findings, it is recommended to take the following factors into account when implementing the approach proposed in this study:

(1) if missing data is relatively scarce, using the coordinate values of the nearest non-missing point to replace random noise data as an input for the generator model may yield positive results. The distance measurement can be based on the node distance of the graph structure transformed from the human posture connection relationship.

(2) when normalizing data with missing values, it is crucial to increase the normalization interval appropriately based on the missing data. This can prevent real coordinates from going

out of bounds and causing the generator model, which uses sigmoid function as its output layer, to generate inaccurate data.

It should be noted that there are still limitations and opportunities for further research. Due to limited dataset availability, the number of complete pedestrian pose data used for GAN training was relatively small, which constrained the performance of SDR-GAIN. Typically, generative models require a vast amount of data for training, so larger or specialized datasets may enhance SDR-GAIN's performance.

REFERENCES

- [1] Severino, J. V. B., Zimmer, A., Brandmeier, T., & Freire, R. Z. (2019). Pedestrian recognition using micro Doppler effects of radar signals based on machine learning and multi-objective optimization. *Expert Systems with Applications*, 136, 304-315.
- [2] Chen, S., Chen, Y., Zhang, S., & Zheng, N. (2019). A novel integrated simulation and testing platform for self-driving cars with hardware in the loop. *IEEE Transactions on Intelligent Vehicles*, 4(3), 425-436.
- [3] Muhammad, K., Ullah, A., Lloret, J., Del Ser, J., & de Albuquerque, V. H. C. (2020). Deep learning for safe autonomous driving: Current challenges and future directions. *IEEE Transactions on Intelligent Transportation Systems*, 22(7), 4316-4336.
- [4] Kashihara, K. (2017, October). Deep Q learning for traffic simulation in autonomous driving at a highway junction. In 2017 IEEE International Conference on Systems, Man, and Cybernetics (SMC) (pp. 984-988). IEEE.
- [5] Camara, F., Bellotto, N., Cosar, S., Nathanael, D., Althoff, M., Wu, J., ... & Fox, C. W. (2020). Pedestrian models for autonomous driving Part I: low-level models, from sensing to tracking. *IEEE Transactions on Intelligent Transportation Systems*, 22(10), 6131-6151.
- [6] Alvarez, W. M., Moreno, F. M., Sipele, O., Smirnov, N., & Olaverri-Monreal, C. (2020, October). Autonomous driving: Framework for pedestrian intention estimation in a real world scenario. In 2020 IEEE Intelligent Vehicles Symposium (IV) (pp. 39-44). IEEE.
- [7] Zhan, H., Liu, Y., Cui, Z., & Cheng, H. (2019, October). Pedestrian detection and behavior recognition based on vision. In 2019 IEEE Intelligent Transportation Systems Conference (ITSC) (pp. 771-776). IEEE.
- [8] Varytimidis, D., Alonso-Fernandez, F., Duran, B., & Englund, C. (2018, November). Action and intention recognition of pedestrians in urban traffic. In 2018 14th International conference on signal-image technology & internet-based systems (SITIS) (pp. 676-682). IEEE.
- [9] Kim, U. H., Ka, D., Yeo, H., & Kim, J. H. (2020). A real-time vision framework for pedestrian behavior recognition and intention prediction at intersections using 3d pose estimation. *arXiv preprint arXiv:2009.10868*.
- [10] Schulz, A. T., & Stiefelwagen, R. (2015, June). Pedestrian intention recognition using latent-dynamic conditional random fields. In 2015 IEEE Intelligent Vehicles Symposium (IV) (pp. 622-627). IEEE.
- [11] Wang, H., Wang, B., Liu, B., Meng, X., & Yang, G. (2017). Pedestrian recognition and tracking using 3D LiDAR for autonomous vehicle. *Robotics and Autonomous Systems*, 88, 71-78.
- [12] Gu, Y., & Kamijo, S. (2014, October). Recognition and pose estimation of urban road users from on-board camera for collision avoidance. In 17th International IEEE Conference on Intelligent Transportation Systems (ITSC) (pp. 1266-1273). IEEE.
- [13] Geismann, P., & Schneider, G. (2008, June). A two-staged approach to vision-based pedestrian recognition using Haar and HOG features. In 2008 IEEE Intelligent Vehicles Symposium (pp. 554-559). IEEE.
- [14] Bauer, S., Brunsmann, U., & Schlotterbeck-Macht, S. (2009, July). FPGA implementation of a HOG-based pedestrian recognition system. In *Proc. MPC-Workshop* (pp. 49-58).
- [15] Cao, H., Yamaguchi, K., Naito, T., & Ninomiya, Y. (2010). Pedestrian recognition using second-order HOG feature. In *Computer Vision-ACCV 2009: 9th Asian Conference on Computer Vision*, Xi'an,

- September 23-27, 2009, Revised Selected Papers, Part II 9 (pp. 628-634). Springer Berlin Heidelberg.
- [16] Dow, Chyi-Ren, et al. "A crosswalk pedestrian recognition system by using deep learning and zebra-crossing recognition techniques." *Software: Practice and Experience* 50.5 (2020): 630-644.
- [17] Zhao, L., & Thorpe, C. E. (2000). Stereo-and neural network-based pedestrian detection. *IEEE Transactions on intelligent transportation systems*, 1(3), 148-154.
- [18] Pop, D. O., Rogozan, A., Nashashibi, F., & Benshair, A. (2017, June). Incremental cross-modality deep learning for pedestrian recognition. In *2017 IEEE Intelligent Vehicles Symposium (IV)* (pp. 523-528). IEEE.
- [19] Wagner, T., Feger, R., & Stelzer, A. (2015, September). Modification of DBSCAN and application to range/Doppler/DoA measurements for pedestrian recognition with an automotive radar system. In *2015 European Radar Conference (EuRAD)* (pp. 269-272). IEEE.
- [20] Bartsch, A., Fitzek, F., & Rasshofer, R. H. (2012). Pedestrian recognition using automotive radar sensors. *Advances in Radio Science*, 10(B. 2), 45-55.
- [21] Pech, A. H., Nauth, P. M., & Michalik, R. (2019, July). A new approach for pedestrian detection in vehicles by ultrasonic signal analysis. In *IEEE EUROCON 2019-18th International Conference on Smart Technologies* (pp. 1-5). IEEE.
- [22] Kidono, Kiyosumi, Takashi Naito, and Jun Miura. "Reliable pedestrian recognition combining high-definition lidar and vision data." *2012 15th international IEEE conference on intelligent transportation systems*. IEEE, 2012.
- [23] Guo, X. P., Du, J. S., Gao, J., & Wang, W. (2018, August). Pedestrian detection based on fusion of millimeter wave radar and vision. In *Proceedings of the 2018 International Conference on Artificial Intelligence and Pattern Recognition* (pp. 38-42).
- [24] Braun, M., Krebs, S., Flohr, F., & Gavrilu, D. M. (2019). Eurocity persons: A novel benchmark for person detection in traffic scenes. *IEEE transactions on pattern analysis and machine intelligence*, 41(8), 1844-1861.
- [25] Xu, H., Guo, M., Nedjah, N., Zhang, J., & Li, P. (2022). Vehicle and pedestrian detection algorithm based on lightweight YOLOv3-promote and semi-precision acceleration. *IEEE Transactions on Intelligent Transportation Systems*, 23(10), 19760-19771.
- [26] Dollar, P., Wojek, C., Schiele, B., & Perona, P. (2011). Pedestrian detection: An evaluation of the state of the art. *IEEE transactions on pattern analysis and machine intelligence*, 34(4), 743-761.
- [27] Xiao, Y., Zhou, K., Cui, G., Jia, L., Fang, Z., Yang, X., & Xia, Q. (2021). Deep learning for occluded and multi-scale pedestrian detection: A review. *let Image Processing*, 15(2), 286-301.
- [28] Dominguez-Sanchez, A., Cazorla, M., & Orts-Escolano, S. (2017). Pedestrian movement direction recognition using convolutional neural networks. *IEEE transactions on intelligent transportation systems*, 18(12), 3540-3548.
- [29] Lingqiu, Z., Jisen, M., Qingwen, H., & Lei, Y. (2020). A Pedestrian Hazard Assessment Method in Urban Road Scene. *Journal of Hunan University Natural Sciences*, 47(8).
- [30] Papandreou, G., Zhu, T., Kanazawa, N., Toshev, A., Tompson, J., Bregler, C., & Murphy, K. (2017). Towards accurate multi-person pose estimation in the wild. In *Proceedings of the IEEE conference on computer vision and pattern recognition* (pp. 4903-4911).
- [31] Fang, H. S., Xie, S., Tai, Y. W., & Lu, C. (2017). Rmpe: Regional multi-person pose estimation. In *Proceedings of the IEEE international conference on computer vision* (pp. 2334-2343).
- [32] Insafutdinov, E., Pishchulin, L., Andres, B., Andriluka, M., & Schiele, B. (2016). Deepercut: A deeper, stronger, and faster multi-person pose estimation model. In *Computer Vision–ECCV 2016: 14th European Conference, Amsterdam, The Netherlands, October 11-14, 2016, Proceedings, Part VI 14* (pp. 34-50). Springer International Publishing.
- [33] Wei, S. E., Ramakrishna, V., Kanade, T., & Sheikh, Y. (2016). Convolutional pose machines. In *Proceedings of the IEEE conference on Computer Vision and Pattern Recognition* (pp. 4724-4732).
- [34] Cao, Z., Simon, T., Wei, S. E., & Sheikh, Y. (2017). Realtime multi-person 2d pose estimation using part affinity fields. In *Proceedings of the IEEE conference on computer vision and pattern recognition* (pp. 7291-7299).
- [35] Cheng, B., Xiao, B., Wang, J., Shi, H., Huang, T. S., & Zhang, L. (2020). Higherhrnet: Scale-aware representation learning for bottom-up human pose estimation. In *Proceedings of the IEEE/CVF conference on computer vision and pattern recognition* (pp. 5386-5395).
- [36] Li, F., Fan, S., Chen, P., & Li, X. (2020, October). Pedestrian motion state estimation from 2D pose. In *2020 IEEE Intelligent Vehicles Symposium (IV)* (pp. 1682-1687). IEEE.
- [37] Xu, F., Xu, F., Xie, J., Pun, C. M., Lu, H., & Gao, H. (2021). Action recognition framework in traffic scene for autonomous driving system. *IEEE Transactions on Intelligent Transportation Systems*, 23(11), 22301-22311.
- [38] Wang, Z., & Papanikolopoulos, N. (2020, October). Estimating pedestrian crossing states based on single 2D body pose. In *2020 IEEE/RSJ International Conference on Intelligent Robots and Systems (IROS)* (pp. 2205-2210). IEEE.
- [39] Zhang, X., Angeloudis, P., & Demiris, Y. (2022). ST CrossingPose: A Spatial-Temporal Graph Convolutional Network for Skeleton-Based Pedestrian Crossing Intention Prediction. *IEEE Transactions on Intelligent Transportation Systems*, 23(11), 20773-20782.
- [40] Zhang, S., Abdel-Aty, M., Wu, Y., & Zheng, O. (2021). Pedestrian crossing intention prediction at red-light using pose estimation. *IEEE Transactions on Intelligent Transportation Systems*, 23(3), 2331-2339.
- [41] Quintero, R., Parra, I., Llorca, D. F., & Sotelo, M. A. (2015, September). Pedestrian intention and pose prediction through dynamical models and behaviour classification. In *2015 IEEE 18th International Conference on Intelligent Transportation Systems* (pp. 83-88). IEEE.
- [42] Fang, Z., & López, A. M. (2018, June). Is the pedestrian going to cross? answering by 2d pose estimation. In *2018 IEEE intelligent vehicles symposium (IV)* (pp. 1271-1276). IEEE.
- [43] Cadena, P. R. G., Yang, M., Qian, Y., & Wang, C. (2019, October). Pedestrian graph: Pedestrian crossing prediction based on 2d pose estimation and graph convolutional networks. In *2019 IEEE Intelligent Transportation Systems Conference (ITSC)* (pp. 2000-2005). IEEE.
- [44] Marginean, A., Brehar, R., & Negru, M. (2019, October). Understanding pedestrian behaviour with pose estimation and recurrent networks. In *2019 6th International Symposium on Electrical and Electronics Engineering (ISEEE)* (pp. 1-6). IEEE.
- [45] Zhou, C., & Yuan, J. (2017). Learning to integrate occlusion-specific detectors for heavily occluded pedestrian detection. In *Computer Vision–ACCV 2016: 13th Asian Conference on Computer Vision, Taipei, Taiwan, November 20-24, 2016, Revised Selected Papers, Part II 13* (pp. 305-320). Springer International Publishing.
- [46] Ouyang, W., Zeng, X., & Wang, X. (2015). Partial occlusion handling in pedestrian detection with a deep model. *IEEE Transactions on Circuits and Systems for Video Technology*, 26(11), 2123-2137.
- [47] Mathias, M., Benenson, R., Timofte, R., & Van Gool, L. (2013). Handling occlusions with franken-classifiers. In *Proceedings of the IEEE International Conference on Computer Vision* (pp. 1505-1512).
- [48] Zhang, S., Yang, J., & Schiele, B. (2018). Occluded pedestrian detection through guided attention in cnns. In *Proceedings of the IEEE conference on Computer Vision and Pattern Recognition* (pp. 6995-7003).
- [49] Kishore, P. S. R., Das, S., Mukherjee, P. S., & Bhattacharya, U. (2019). ClueNet: A Deep Framework for Occluded Pedestrian Pose Estimation. In *BMVC* (p. 245).
- [50] Goodfellow, I., Pouget-Abadie, J., Mirza, M., Xu, B., Warde-Farley, D., Ozair, S., Courville, A., & Bengio, Y. (2014). Generative adversarial nets. *Advances in Neural Information Processing Systems* (pp. 2672-2680).
- [51] Yoon, J., Jordon, J., & Schaar, M. (2018, July). Gain: Missing data imputation using generative adversarial nets. In *International conference on machine learning* (pp. 5689-5698). PMLR.
- [52] Ho, J., Jain, A., & Abbeel, P. (2020). Denoising diffusion probabilistic models. *Advances in Neural Information Processing Systems*, 33, 6840-6851.

- [53] Mattei, P. A., & Frellsen, J. (2019, May). MIWAE: Deep generative modelling and imputation of incomplete data sets. In *International conference on machine learning* (pp. 4413-4423). PMLR.
- [54] Zhang, Y., Zhou, B., Cai, X., Guo, W., Ding, X., & Yuan, X. (2021). Missing value imputation in multivariate time series with end-to-end generative adversarial networks. *Information Sciences*, 551, 67-82.
- [55] Xu, Y., Zhang, Z., You, L., Liu, J., Fan, Z., & Zhou, X. (2020). sclGANs: single-cell RNA-seq imputation using generative adversarial networks. *Nucleic acids research*, 48(15), e85-e85.
- [56] Cao, Z., Hidalgo, G., Simon, T., Wei, S. E., & Sheikh, Y. (2021). OpenPose: realtime multi-person 2D pose estimation using Part Affinity Fields. *IEEE transactions on pattern analysis and machine intelligence*, 43(1), 172-186.
- [57] Mangalam, K., Adeli, E., Lee, K. H., Gaidon, A., & Niebles, J. C. (2020). Disentangling human dynamics for pedestrian locomotion forecasting with noisy supervision. In *Proceedings of the IEEE/CVF Winter Conference on Applications of Computer Vision* (pp. 2784-2793).
- [58] Kwan-Loo, K. B., Ortíz-Bayliss, J. C., Conant-Pablos, S. E., Terashima-Marín, H., & Rad, P. (2022). Detection of violent behavior using neural networks and pose estimation. *IEEE Access*, 10, 86339-86352.
- [59] Walocha, F., Drewitz, U., & Ihme, K. (2022). Activity and Stress Estimation Based on OpenPose and Electrocardiogram for User-Focused Level-4-Vehicles. *IEEE Transactions on Human-Machine Systems*, 52(4), 538-546.
- [60] Li, Y., Dogan, A., & Liu, C. (2022, August). Ensemble Generative Adversarial Imputation Network with Selective Multi-Generator (ESM-GAIN) for Missing Data Imputation. In *2022 IEEE 18th International Conference on Automation Science and Engineering (CASE)* (pp. 807-812). IEEE.
- [61] Zhou, X., Liu, X., Lan, G., & Wu, J. (2021). Federated conditional generative adversarial nets imputation method for air quality missing data. *Knowledge-Based Systems*, 228, 107261.
- [62] He, K., Zhang, X., Ren, S., & Sun, J. (2016). Deep residual learning for image recognition. In *Proceedings of the IEEE conference on computer vision and pattern recognition* (pp. 770-778).
- [63] Lin, T. Y., Maire, M., Belongie, S., Hays, J., Perona, P., Ramanan, D., ... & Zitnick, C. L. (2014). Microsoft coco: Common objects in context. In *Computer Vision—ECCV 2014: 13th European Conference, Zurich, Switzerland, September 6-12, 2014, Proceedings, Part V 13* (pp. 740-755). Springer International Publishing.
- [64] Kotseruba, I., Rasouli, A., & Tsotsos, J. K. (2016). Joint attention in autonomous driving (JAAD). *arXiv preprint arXiv:1609.04741*.
- [65] Zhao, S., Li, H., Ke, Q., Liu, L., & Zhang, R. (2021). Action-vit: Pedestrian intent prediction in traffic scenes. *IEEE Signal Processing Letters*, 29, 324-328.
- [66] Sun, C., Chen, Y., & Cheng, C. (2021). Imputation of missing data from offshore wind farms using spatio-temporal correlation and feature correlation. *Energy*, 229, 120777.
- [67] Dan, E. L., Dînşoreanu, M., & Mureşan, R. C. (2020, May). Accuracy of six interpolation methods applied on pupil diameter data. In *2020 IEEE international conference on automation, quality and testing, robotics (AQTR)* (pp. 1-5). IEEE.
- [68] Malarvizhi, R., & Thanamani, A. S. (2012). K-nearest neighbor in missing data imputation. *Int. J. Eng. Res. Dev*, 5(1), 5-7.
- [69] Stekhoven, D. J., & Bühlmann, P. (2012). MissForest—non-parametric missing value imputation for mixed-type data. *Bioinformatics*, 28(1), 112-118.
- [70] Payre, W., Cestac, J., & Delhomme, P. (2016). Fully automated driving: Impact of trust and practice on manual control recovery. *Human factors*, 58(2), 229-241.
- [71] Jiao, Y., Yao, H., & Xu, C. (2020). PEN: Pose-embedding network for pedestrian detection. *IEEE Transactions on Circuits and Systems for Video Technology*, 31(3), 1150-1162.
- [72] Cosma, A., Radoi, I. E., & Radu, V. (2019, September). Camloc: Pedestrian location estimation through body pose estimation on smart cameras. In *2019 International Conference on Indoor Positioning and Indoor Navigation (IPIN)* (pp. 1-8). IEEE.